Intercalation of Cu^{2+} in the $HNiPO_4 \cdot H_2O$ Layered Phosphate: Study of the Structure, Spectroscopic, and Magnetic Properties of the Intercalated Derivative and the Related $CuNi_2(PO_4)_2$ Compound

Aintzane Goñi,[†] Luis Lezama,[†] José Luis Pizarro,[‡] Jaione Escobal,[†] María Isabel Arriortua,[‡] and Teófilo Rojo*[,†]

Departamento de Química Inorgánica and Departamento de Mineralogía y Petrología, Universidad del País Vasco, Bilbao 48080, Spain

Received December 29, 1998. Revised Manuscript Received April 12, 1999

A Cu(II) intercalated phase was obtained from the insertion of Cu(II) ions in the $HNiPO_4 \cdot H_2O$ layered phosphate. This phase was characterized by using XRD, analytical, and spectroscopic techniques. The intercalation process does not introduce any significant change in the structure of the nickel phosphate layers. However, the distance between layers shows an increase induced by the homogeneous distribution of the Cu(II) ions in the interlayer space. The $CuNi_2(PO_4)_2$ heterometallic phosphate was obtained from the thermal treatment of the Cu(II) intercalated compound. $CuNi_2(PO_4)_2$ crystallizes in the monoclinic $P2_1/n$ space group, with cell parameters $a = 6.393(1)$, $b = 9.325(1)$, and $c = 4.718(1)$ Å; $\beta = 90.71(1)°$; $V = 281.24$ Å^3; and $Z = 2$. The three-dimensional structure is built by corner-sharing PO_4 tetrahedra, CuO_4 planar squares, and Ni_2O_8 dimers. The Ni(II) ions exhibit, in this compound, an unusual five-coordination with a geometry intermediate between trigonal bipyramid and square-planar pyramid but slightly closer to the latter disposition. ESR and magnetic measurements for the intercalated derivative and the $CuNi_2(PO_4)_2$ compound suggest the presence of magnetic couplings of long-range order between the Cu(II) and Ni(II) ions in both cases. The layered intercalated derivative shows an antiferromagnetic three-dimensional behavior in which the interlayer magnetic interactions are established through the inserted Cu(II) ions. In the case of the $CuNi_2(PO_4)_2$ phase, a global antiferromagnetic ordering is observed with a transitory ferrimagnetic behavior in the 75−40 K temperature range due to the spin decompensation of the coupled Cu(II) and Ni(II) ions present in the structure.

Introduction

The intercalation process is being considered as a way to obtain new materials with specially structural characteristics and predetermined physical and chemical properties.[1] That is the purpose of the introduction of magnetic cations such as Co^{2+}, Ni^{2+}, or Cu^{2+} inside the layered structure of some phosphate compounds. The intercalation can produce interesting changes in the magnetic behavior of the matrix phases,[2,3] making it possible to use some techniques such as ESR spectroscopy or magnetic susceptibility measurements for determining magneto-structural correlations between the layered host-net and the intercalated guests. That information is very important in order to develop and improve the applications of the materials.

The intercalation studies of Ni^{2+} and Co^{2+} in the layered phosphate $VOPO_4 \cdot 2H_2O$ showed the formation of lineal bridges of the type V═O−M−O═V (M = Co^{2+} and Ni^{2+}) between the vanadyl phosphate layers, arranging the bridges perpendicularly to phosphate sheets.[4] This ordering allows an efficient interlayer magnetic exchange. However, when the intercalated ion was Cu^{2+}, a square-planar coordination was observed for this cation in the interlayer space, arranging parallel to the vanadyl phosphate layers.[5] The insertion of cobalt and nickel hydroxyacetates inside the layers of α-$Zr(HPO_4)_2 \cdot H_2O$ gave rise to the attainment of a composite compound in which the zirconium phosphate sheets were alternating with layers of the magnetic atoms linked by hydroxo and acetate bridges. By heating to 700 K, the metallic hydroxyacetate sheets became nickel or cobalt oxide layers showing the resulting composite interesting ferromagnetic properties.[6]

The layered nickel phosphate, $HNiPO_4 \cdot H_2O$, obtained by deintercalation of the ammonium groups from the $NH_4NiPO_4 \cdot H_2O$[7] phase, was used as the intercalation matrix. The capacity to insert different alkylamines in

* To whom all correspondence should be addressed. E-mail: qiproapt@lg.ehu.es. Fax: 34-94-4648500. Phone: 34-94-6012000.
[†] Departamento de Química Inorgánica.
[‡] Departamento de Mineralogía y Petrología.

(1) Schöllhorn, R. *Chem. Mater.* **1996**, *8*, 1747.
(2) Antonio, M. R.; Barbour, R. L.; Blum, P. R. *Inorg. Chem.* **1987**, *26*, 1235.
(3) Papoutsakis, D.; Jackson, J. E.; Nocera, D. G. *Inorg. Chem.* **1996**, *35*, 800.
(4) Haushalter, R. C.; Soghomonian, V.; Chen, Q.; Zubieta, J. *J. Solid State Chem.* **1993**, *105*, 512.
(5) Zhang, Y.; Clearfield, A.; Haushalter, R. C. *J. Solid State Chem.* **1995**, *117*, 157.
(6) Shpeizer, B.; Poojary, D. M.; Ahn, K.; Runyan, C. E.; Clearfield, A. *Science* **1994**, *266*, 1357.

10.1021/cm980785w CCC: $18.00
Published on Web 06/19/1999

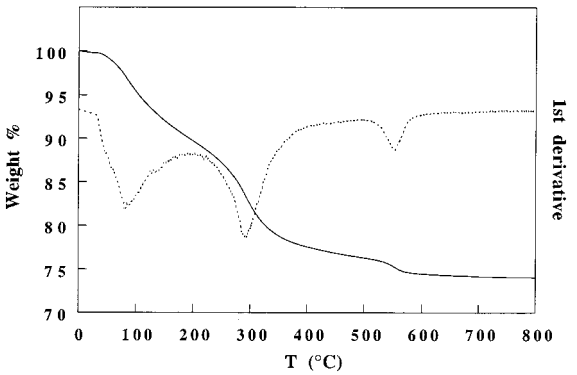

Figure 1. TGA and DTG curves of the Cu(II) intercalated derivative of $HNiPO_4 \cdot H_2O$.

the interlayer space by a topotactic reversible acid−base reaction was verified,[8] and this phase together with the alkylamine intercalated derivatives $(C_nH_{n+1}NH_2)_x$-$HNiPO_4 \cdot H_2O$ showed interesting properties. The ability of the layered $HNiPO_4 \cdot H_2O$ phosphate for intercalation is limited by the existence of hydrogen bonds between the sheets, which makes the diffusion of the guest species across the interlayer space difficult. However, the formation, in the first step, of an intermediate intercalated phase by inserting alkylamines could give rise to an increase in the interlayer space favoring the intercalation of a larger diversity of guest species.[9]

In this paper, we present the insertion of Cu^{2+} cationic species between the layers of the $HNiPO_4 \cdot H_2O$ compound to obtain a heterometallic intercalation derivative. The resulting compound has been calcined, giving rise to the formation of the new $CuNi_2(PO_4)_2$ phase, which shows a crystal structure related to that observed for the $Cu_3(PO_4)_2$ compound[10] and exhibits interesting spectroscopic and magnetic properties.

Experimental Section

Synthesis and Characterization of the Cu(II) Intercalated Derivative of $HNiPO_4 \cdot H_2O$. To facilitate the insertion of Cu(II) species in the $HNiPO_4 \cdot H_2O$ layered phase, the intercalation of hexylamine was previously carried out by using the method described in ref 8. This hexylamine intercalated intermediate with yellow color was analyzed, characterized, and then added to a 0.025 M methanolic solution of $Cu(CH_3COO)_2 \cdot H_2O$ and $Cu(NO_3)_2 \cdot 3H_2O$. The solid−liquid mixture was stirred at room temperature for 1 week. After this time, the solid was recovered and added to another similar just prepared solution. Finally, the solid of green color was filtered, washed with methanol and acetone, and dried in air. The experimental results of the content of Ni, Cu, P, C, N and H were as follows: Ni = 24.3%, Cu = 11.8%, P = 12.8%, C = 4.0%, and H = 3.0%. Presence of N was not detected in the sample, indicating the total deintercalation of the hexylamine employed in the intermediate step.

Thermogravimetric measurements were carried out by heating the sample at 10°/min in the range from room temperature to 800 °C in nitrogen atmosphere. The results are given in Figure 1. The thermal analysis showed a total mass loss equivalent to 25% of the initial mass. The weight loss takes place progressively in all temperature ranges. However, three different overlapped steps could be considered. The first one would occur from room temperature to around 180 °C (mass loss 10%), and it could be attributed to the evaporation of approximately 1.5 mol of methanol/mol of compound (theoretical weight 9.91%). The presence of methanol in the compound is probably due to the insertion of a portion of solvent in the interlayer space during the intercalation process being weakly linked to the inorganic matrix.

The second step takes place at 180 °C and corresponds to the loss of water molecules, probably coordinated to the metal ions. This step continues up to 400 °C and originates a mass loss of 14%, in good agreement with the existence of four water molecules per formula, two for each inserted Cu(II) ion and one for each Ni(II) ion, as occurred in the $HNiPO_4 \cdot H_2O$ precursor. Finally, the last decomposition step observed at higher temperatures corresponding to a mass loss of 1.5% could be attributed to the disappearance of a small amount of phosphorus as P_2O_5.

The above results together with those obtained from the structural characterization, described below, allow us to propose $Cu_{0.9}Ni_2(PO_4)_{1.8}(HPO_4)_{0.2} \cdot 4H_2O \cdot 1.5CH_3OH$ as the most plausible formula for the synthesized compound.

Synthesis of $CuNi_2(PO_4)_2$. The $CuNi_2(PO_4)_2$ phase was prepared by heating the intercalated $Cu_{0.9}Ni_2(PO_4)_{1.8}(HPO_4)_{0.2} \cdot 4H_2O \cdot 1.5CH_3OH$ compound at 800 °C for 3 h in air atmosphere. Similar results were obtained in nitrogen atmosphere. The final product was washed with water and acetone and dried in air. The experimental contents of Cu, Ni, and P in the sample were as follows: Cu = 17.7%, Ni = 32.8%, and P = 16.7%. Calculated: Cu = 17.1%, Ni = 31.7%, and P = 16.7%.

Characterization and Physical Measurements. Microanalyses were performed with a Perkin-Elmer 2400 CHN analyzer. Analytical measurements were carried out by inductively coupled plasma atomic emission spectroscopy (ICP-AES) analysis, with an ARL 3410+ICP with Minitorch equipment. X-ray diffraction patterns of the $Cu_{0.9}Ni_2(PO_4)_{1.8}(HPO_4)_{0.2} \cdot 4H_2O \cdot 1.5CH_3OH$ and $CuNi_2(PO_4)_2$ compounds were recorded on a Stoe diffractometer, using transmission geometry and Cu $K\alpha_1$ radiation. Infrared spectra were performed with a Nicolet FT-IR 740 spectrometer using the KBr disk technique. Thermogravimetric analysis of the copper intercalated phase was performed with a Perkin-Elmer System-7 DSC-TGA. ESR spectra were carried out in a Bruker ESP 300 spectrometer, operating at Q- and X-band, equipped with a standard Oxford low-temperature device, calibrated by the NMR probe for the magnetic field. and a Hewlett-Packard 5352B frequency counter for the microwave frequency. Magnetic susceptibility measurements were performed at 0.1 T with a Quantum SQUID magnetometer in the 1.8−300 K temperature range.

Results and Discussion

Crystallographic Study of $Cu_{0.9}Ni_2(PO_4)_{1.8}(HPO_4)_{0.2} \cdot 4H_2O \cdot 1.5CH_3OH$. X-ray diffraction pattern of the $Cu_{0.9}Ni_2(PO_4)_{1.8}(HPO_4)_{0.2} \cdot 4H_2O \cdot 1.5CH_3OH$ compound was registered in the 5−70° 2θ range, every 0.02°, and during 10 s per step. As can be observed in Figure 2, the diffraction peaks are very broad and of low intensity. These facts are characteristic of intercalation compounds and could be originated by the disorder generated by the insertion of guest species between the sheets of the layered matrix.[11]

The obtained XRD pattern for this compound was compared with those of the related phases, such as $NH_4NiPO_4 \cdot H_2O$, $HNiPO_4 \cdot H_2O$, and alkylamine derivatives $(C_nH_{2n+1}NH_2)_xHNiPO_4 \cdot H_2O$. A similarity between the patterns of $NH_4NiPO_4 \cdot H_2O$ and the Cu(II) intercalated derivative was observed (see Figure 2). The $HNiPO_4 \cdot H_2O$ intercalation matrix presents a different pattern.

(7) Goñi, A.; Pizarro, J. L.; Lezama, L. M.; Barberis, G. E.; Arriortua, M. I.; Rojo, T. *J. Mater. Chem.* **1996**, *6* (3), 421.
(8) Goñi, A.; Rius, J.; Insausti, M.; Lezama, L. M.; Pizarro, J. L.; Arriortua, M. I.; Rojo, T. *Chem. Mater.* **1996**, *8*, 1052.
(9) Clearfield, A.; Roberts, B. D. *Inorg. Chem.* **1988**, *27*, 3237.
(10) Shoemaker, G. L.; Anderson, J. B.; Kostiner, E. *Acta Crystallogr.* **1977**, *B33*, 2969.
(11) Drits, V. A.; Tchaubar, C. *X-ray Diffraction by Disordered Lamellar Structures*; Springer: New York, 1990.

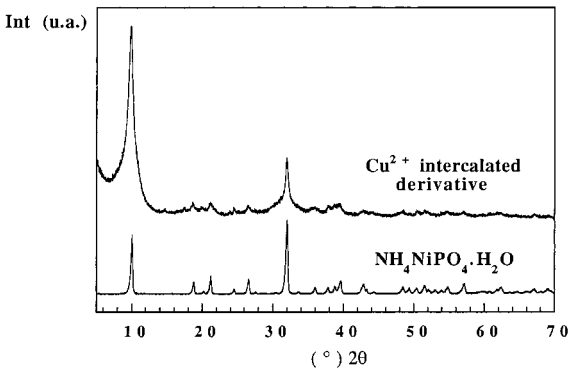

Figure 2. XRD patterns of the Cu(II) intercalated derivative and $NH_4NiPO_4 \cdot H_2O$ related compound.

Unlike the $NH_4NiPO_4 \cdot H_2O$ phase, where the layers are separated by the NH_4^+ cations, in the $HNiPO_4H_2O$ matrix the nickel phosphate sheets are connected by a zigzag system of the hydrogen bonds (see ref 8).

A strong peak appears at low angles in the patterns of the Cu(II) intercalate and the $NH_4NiPO_4 \cdot H_2O$ phase. The *d* value of that peak is attributed to the interlayer distance for each compound. In the $NH_4NiPO_4 \cdot H_2O$ phase, the reflection is located at 10.08° in 2θ ($d = 8.76$ Å), whereas in the Cu^{2+} intercalated derivative, the diffraction maximum is situated at 9.77°, corresponding to an interlayer distance of 9.04 Å. The indexation of the XRD pattern of the Cu(II) intercalated derivative was carried out by using the LSUCREB[12] program, starting from the cell parameters of the $NH_4NiPO_4 \cdot H_2O$ compound. The Cu(II) intercalated phase crystallizes in the orthorhombic system, with the following cell parameters: $a = 5.582(1)$, $b = 9.032(2)$, and $c = 4.724(1)$ Å. The experimental data do not allow the resolution of its crystal structure; however, the similarity of the patterns for this phase and $NH_4NiPO_4 \cdot H_2O$ (see Figure 2) permits us to propose a similar crystal structure without a significant variation of the nickel phosphate layers for these phases (Figure 3). The intercalation and deintercalation processes in this family of compounds are topotactic, and so, modifications in the layer structure of the host matrix are not introduced. These results are in good agreement with those observed in the intercalation processes of different alkylamines in this matrix.[8]

Taking into account the charge difference of the NH_4^+ and Cu^{2+} ions, the latter ions can be described as situated in one-half of the sites corresponding to the NH_4^+ positions in the structure of $NH_4NiPO_4 \cdot H_2O$. Two alternative options for the copper distribution considering the homogeneous situation of the electric charges can be considered (see Figure 3). In the first case (a), each Cu(II) ion should be bonded to only one phosphate group, with a Cu−O bond distance around 2.0 Å. The Cu(II) ions could be semicoordinated to one water molecule belonging to the adjacent layer, situated at a distance of approximately 3.0 Å. Each Cu(II) ion probably bonds to other two water molecules, located in the interlayer space, being the coordination number for the Cu(II) ion 3 + 1 with three short and one long Cu−O distances. In the second case (b), the copper ions would

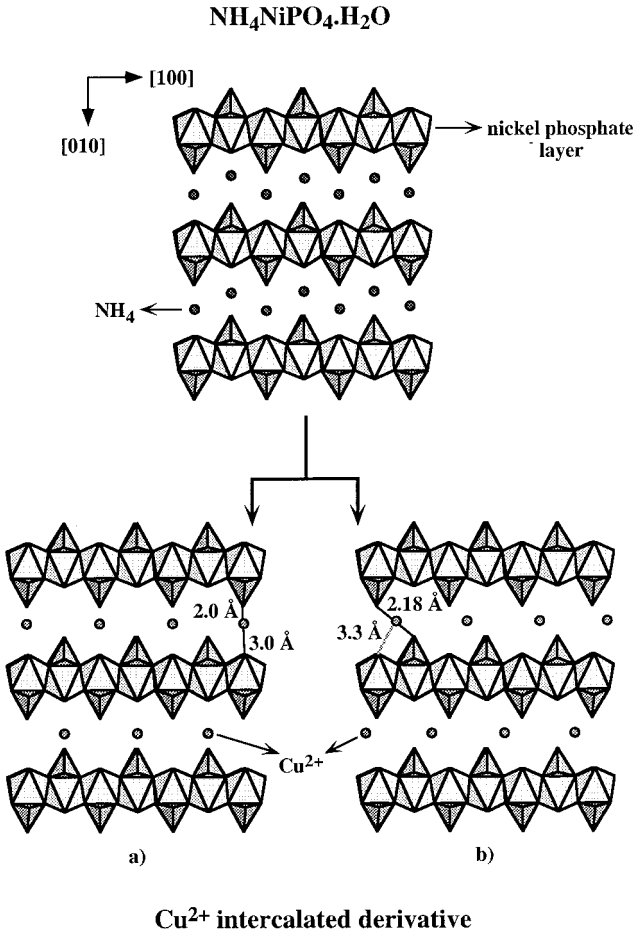

Figure 3. Crystal structure of the $NH_4NiPO_4 \cdot H_2O$ compound and two alternative options for the copper distribution in the structure of the Cu(II) intercalated derivative.

act as a bridge between the layers bonding to two phosphate groups of the two adjacent layers, with Cu−O distances near 2.18 Å. The coordination to two water molecules located in the interlayer space together with the semicoordination to one water molecule in a sheet (semicoordination distance ≈ 3.3 Å) would complete the coordination 4 + 1 for the Cu(II) ions, with four short and one long Cu−O distances.

Crystal Structure of $CuNi_2(PO_4)_2$. The crystal structure of $CuNi_2(PO_4)_2$ was performed by using the XRD technique on a polycrystalline sample. The data collection was made in the 10−110° 2θ range, every 0.02° in 2θ, and during 20 s per step. The resolution of the structure was carried out ab initio without considering a structural model. The positions of the most intense reflections in the pattern were used for the indexation by the TREOR[13] program, obtaining a monoclinic cell with parameters $a = 6.398$, $b = 9.332$, and $c = 4.721$ Å and $\beta = 90.70°$. The pattern matching analysis, carried out by the FULLPROF[14] program, allowed the refinement of the cell parameters as well as the profile parameters. During this process, a group of additional weak reflections corresponding to the presence of a small amount of $Ni_3(PO_4)_2$[15] was also observed. This Ni_3-

(12) Appleman, D. E.; Evans, H. T. *LSUCREB, Indexing and Least Square Refinement of Powder Diffraction Data*; U.S. University: Washington, DC, 1973.

(13) Werner, P. E. *TREOR-4 Program;* Arrhenius Laboratory, University of Stockholm: Sweden, 1984.

(14) Rodriguez Carvajal, J. *FULLPROF Program. Rietveld Pattern Matching Analysis of Powder Patterns*; 1994.

(15) Calvo, C.; Faggiani, R. *Can. J. Chem.* **1975**, *53*, 1516.

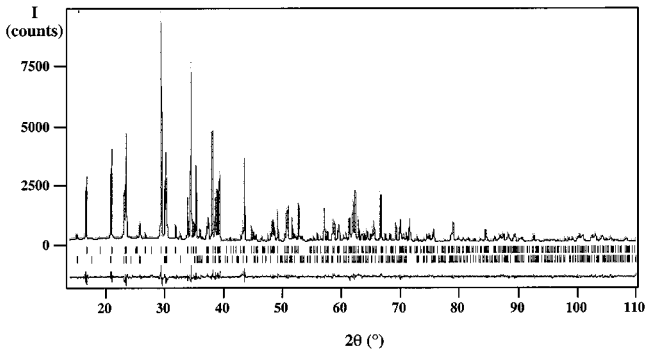

Figure 4. Experimental, calculated, and difference XRD patterns of $CuNi_2(PO_4)_2$.

Table 1. Crystal Parameters and Details of the Structure Refinement of the $CuNi_2(PO_4)_2$ Compound

crystal system	monoclinic
space group (N°)	$P2_1/n$(14)
a (Å)	6.393(1)
b (Å)	9.325(1)
c (Å)	4.718(1)
β (°)	90.71(1)
V (Å^3)	281.24
Z	2
temp (K)	295
diffractometer	STOE
radiation (λ (Å))	$CuK\alpha_1$(1.5406)
2θ (°) range	10−110
step (°)	0.02
time for step (s)	20
structural parameters	26
profile parameters	22
R_F	0.035
R_B	0.045
R_p	0.058
R_{wp}	0.075

$(PO_4)_2$ phase was considered in the subsequent steps of the refinement, introducing its structural model and cycling the corresponding scale factor.

The study of the intensities and systematic extintions for the indexed reflections allowed us to deduce the space group $P2_1/n$ for the $CuNi_2(PO_4)_2$ phase. The final pattern matching analysis with this space group led to the following refined cell parameters: $a = 6.393(1)$, $b = 9.325(1)$, and $c = 4.718(1)$ Å and $\beta = 90.71(1)°$. The integrated intensities of 119 reflections, located between 10 and 70° (2θ), were used to obtain the structure factors for the determination of all the atomic positions by direct methods (SIRPOW[16] program). The resulting structural model was refined by the Rietveld method. The calculated amount of impurity in the sample, characterized as $Ni_3(PO_4)_2$, was 7.6%. The experimental, calculated, and difference XRD patterns of the $CuNi_2(PO_4)_2$ polycrystalline sample are shown in Figure 4. Crystal parameters and details of the data collection and structural refinement are given in Table 1. The bond distances and angles in the structure were calculated using the BONDLA[17] and PARST[18] programs. Tables 2 and 3 show the final atomic coordinates and selected bond distances and angles of $CuNi_2(PO_4)_2$, respectively.

Table 2. Fractional Atomic Coordinates and B_{eq} Temperature Factors (Å^2) for $CuNi_2(PO_4)_2$

atom	x	y	z	B_{eq}
Cu	0.5	0.5	0.5	3.70(4)
Ni	0.6514(2)	0.1239(1)	0.4707(3)	2.93(3)
P	0.6532(4)	0.3201(2)	0.9939(5)	3.26(4)
O(1)	0.3801(8)	0.6768(5)	0.6805(9)	2.78(11)
O(2)	0.8475(7)	0.4175(4)	0.9195(9)	2.63(11)
O(3)	0.6777(6)	0.1643(5)	0.8962(9)	2.81(12)
O(4)	0.4588(7)	0.3858(5)	0.8451(8)	2.62(11)

Table 3. Selected Bond Distances (Å) and Angles (deg) for $CuNi_2(PO_4)_2$[a]

Cu Coordination Planar Square			
Cu−O(1)	2.012(4)	Cu−O(1)^{i}	2.012(4)
Cu−O(4)	1.966(4)	Cu−O(4)^{i}	1.966(4)
O(1)−Cu-O(4)	92.1(2)	O(1)−Cu-O(4)^{i}	87.8(2)
O(1)^{i}−Cu−O(4)^{i}	92.1(2)	O(1)^{i}−Cu−O(4)	87.8(2)
Ni Coordination Polyhedron			
Ni−O(3)	2.048(4)	Ni−O(2)^{ii}	1.993(4)
Ni−O(1)^{i}	2.000(5)	Ni−O(4)^{iii}	2.062(4)
Ni−O(2)^{iv}	1.993(4)		
O(3)−Ni−O(1)^{i}	100.7(2)	O(3)−Ni−O(2)^{ii}	85.6(2)
O(3)−Ni−O(4)^{iii}	102.9(2)	O(3)−Ni−O(2)^{iv}	102.8(2)
O(1)^{i}-Ni−O(2)^{ii}	171.9(2)	O(1)^{i}−Ni−O(4)^{iii}	91.8(2)
O(1)^{i}−Ni−O(2)^{iv}	92.5(2)	O(2)^{ii}−Ni−O(4)^{iii}	91.8(2)
O(2)^{ii}−Ni−O(2)^{iv}	81.1(2)	O(4)^{iii}−Ni−O(2)^{iv}	152.6(2)
Phosphate Tetrahedron			
P−O(1)^{v}	1.554(5)	P−O(2)	1.582(5)
P−O(3)	1.532(5)	P−O(4)	1.546(5)
O(2)−P−O(3)	113.2(3)	O(2)−P−O(4)	107.5(2)
O(2)−P−O(1)^{v}	109.0(3)	O(3)−P−O(4)	108.9(2)
O(3)−P−O(1)^{v}	109.3(3)	O(4)−P−O(1)^{v}	108.8(3)

[a] Symmetry codes: i = $1 - x$, $1 - y$, $1 - z$; ii = $3/2 - x$, $-1/2 + y$, $3/2 - z$; iii = $1/2 + x$, $1/2 - y$, $-1/2 + z$; iv = $-1/2 + x$, $1/2 - y$, $-1/2 + z$; v = $1 - x$, $1 - y$, $2 - z$.

The structure of $CuNi_2(PO_4)_2$ can be described as three-dimensional, being built by three different corner-sharing polyhedra: PO_4 tetrahedra, CuO_4 planar squares, and Ni_2O_8 dimers (Figure 5). The oxygen atoms of the PO_4 groups act as bridges in the structure. The O(1) and O(4) atoms are connecting to the copper(II) and nickel(II) cations (Figure 5a). The O(2) and its symmetric atoms establish the connection between the Ni(II) ions inside the Ni_2O_8 dimers. The O(3) oxygen is only bonded to one Ni(II) ion. Each Ni_2O_8 dimer is linked to the adjacent dimers through the PO_4 groups. The CuO_4 planar square entities do not present direct connection between them and are corner-sharing the Ni_2O_8 dimers (Figure 5b).

It is to note the presence of five-coordinated Ni(II) ions in the $CuNi_2(PO_4)_2$ phase (Figure 6). This coordination is unusual for these ions, and only a few number of compounds exhibiting this coordination has been found.[19−21] The polyhedron of the Ni(II) ions in $CuNi_2(PO_4)_2$ shows Ni−O bond distances ranging from 1.993(4) to 2.062(4) Å and O−Ni−O angles from 81.1(2) to 152.6(2)°. The polyhedron distortion parameter, Δ, has been calculated using the model developed by Muetterties and Guggenberger.[22] The obtained value $\Delta = 0.52$ is intermediate between those corresponding to the regular square planar pyramid ($\Delta = 1$) and the trigonal bipyramid (Δ

(16) Altamontem, A.; Cascarano, G.; Giacovazzo, C.; Guagliardi, A.; Burla, M. C.; Polidori, G.; Camalli, M. *J. Appl. Crystallogr.* **1994**, *27*, 435.
(17) Stewart, J. M.; Kundell, F. A.; Baldwin, J. C. *The XRAY70 SYSTEM*; Computer Science Center, University of Maryland: College Park, MD, 1970.
(18) Nardelli, M. *Comput. Chem.* **1983**, *7*, 95.
(19) Basolo, F.; Pearson, R. G. *Mechanisms of Inorganic Reactions*; John Wiley & Sons: New York, 1967.
(20) Lukaszewicz, K. *Bull. Acad. Pol. Sci.* **1967**, *47*, 51.
(21) Galoisy, L.; Calas, G. *Mater. Res. Bull.* **1993**, *28*, 221.
(22) Muetterties, E. L.; Guggenberger, L. J. *J. Am. Chem. Soc.* **1974**, *96*, 1748.

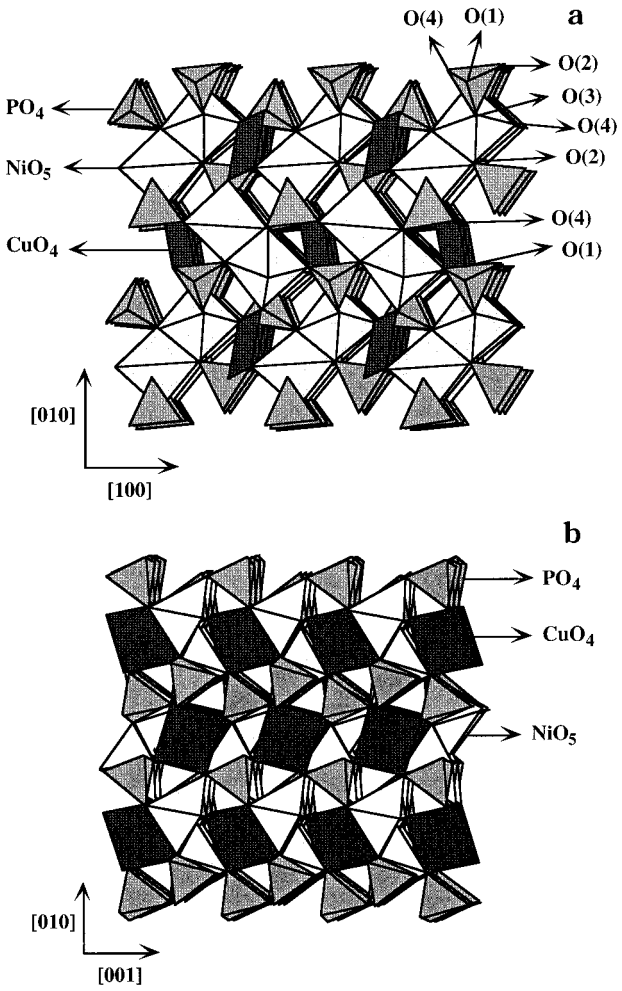

Figure 5. Crystal structure of the $CuNi_2(PO_4)_2$ compound.

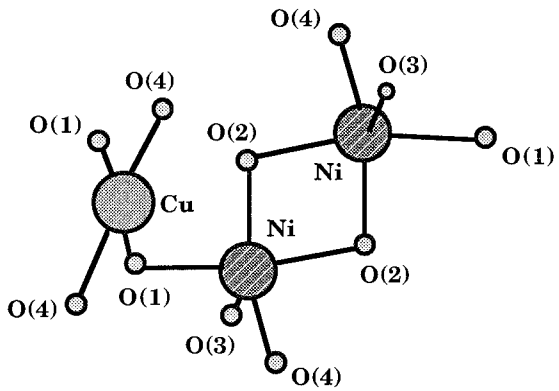

Figure 6. Cu(II) and Ni(II) coordination polyhedra in the structure of $CuNi_2(PO_4)_2$.

= 0). So, the geometry of the polyhedron can be considered as intermediate between trigonal bipyramid and square-planar pyramid being slightly closer to the latter geometry.

The coordination polyhedron of the Cu(II) ion is square planar with a slight rhombic distortion (see Figure 6). The Cu−O distances show two different values, 2.012(4) and 1.966(4) Å, and the O−Cu−O angles are slightly deflected from the ideal value of 90°. It is also interesting to note the radial distortion observed for the PO_4 tetrahedra. The P−O distances range from 1.532(5) Å (distance observed for the P−O(3) bond) to a maximum value of 1.582(5) Å (corresponding to the P−O(2) bond). This fact is probably due to the different coordination numbers of the oxygen atoms, as was described above. The angular distortion of the PO_4 groups is rather small showing no correlation to the radial distortion.

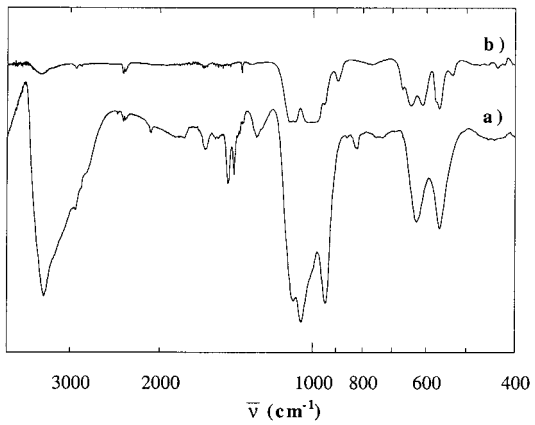

Figure 7. IR spectra of the (a) Cu(II) intercalated derivative and (b) $CuNi_2(PO_4)_2$ compound.

The crystal structure of $CuNi_2(PO_4)_2$ shows a relationship with that corresponding to the $Cu_3(PO_4)_2$ compound,[10] which crystallizes in the triclinic system. In the $Cu_3(PO_4)_2$ phase, the Cu(II) ions occupy two independent positions in the crystal structure. One of them Cu(1) is on a symmetry center. In this site the Cu(II) ion is surrounded by four oxygens forming a slightly distorted planar square geometry. The other site, Cu(2), is in a general position inside a distorted square-planar pyramid, which is edge-shared with other symmetrical pyramid, forming a dimer of the Cu_2O_8 type. The main differences in the topology of the $Cu_3(PO_4)_2$ and $CuNi_2(PO_4)_2$ phases are due to the relative orientations between the dimeric entities. In this way, in the $CuNi_2(PO_4)_2$ phase the Ni_2O_8 dimers are rotated approximately 90° each other along the crystallographic [110] directions, whereas in the $Cu_3(PO_4)_2$ phase the Cu_2O_8 dimers are aligned along the [011] direction from its triclinic cell.[10] However, the $Ni_3(PO_4)_2$ phase shows a quite different crystal structure in which the Ni(II) ions occupy two octahedral sites.[15] The $CuNi_2(PO_4)_2$ phase with a ratio Ni/Cu of 2:1 has adopted a structure related to the anhydrous copper phosphate and not corresponding to the anhydrous nickel phosphate, forcing the Ni(II) ions to be located in an unusual five-coordinated geometry.

Infrared Spectroscopy. The IR spectra of the intercalated and $CuNi_2(PO_4)_2$ compounds were registered in the 400−4000 cm^{-1} wavenumber range (Figure 7). In the case of $Cu_{0.9}Ni_2(PO_4)_{1.8}(HPO_4)_{0.2}\cdot 4H_2O\cdot 1.5CH_3OH$, the IR spectrum shows a broad, strong, and split band in the 3500−3000 cm^{-1} region. This band can be attributed to the stretching vibration mode of the O−H bonds, ν(O−H), of different water and methanol molecules. In the same region and centered at 2930−2900 cm^{-1}, other less intense absorption bands appear practically overlapped, which correspond to the stretching vibration modes of the C−H bonds, ν(C−H), from the methanol molecules. A weak and broad peak is observed at approximately 1635 cm^{-1}, which can be attributed to the bending mode δ(O−H). The bands at 1470 and 1440 cm^{-1} could be assigned to the $\delta(CH_3)$ mode from

methanol molecules. The strong and split peak centered at 1000 cm^{-1} could correspond to the stretching vibration mode of the PO_4 tetrahedra,[23] $\nu(PO_4)$. The absorption profile for this band is similar to that observed for the $NH_4NiPO_4 \cdot H_2O$ compound. This fact is indicative of the existence of similar distortions in the PO_4 groups of both compounds and is confirmed for the presence of a band of medium intensity, located at around 600 cm^{-1}. This band shows a similar splitting to that found for the related band in $NH_4NiPO_4 \cdot H_2O$, corresponding to the bending mode of the phosphate tetrahedra, $\delta(PO_4)$. The stretching vibration mode of the C−O bond from the methanol molecules is not observed, probably due to that band is obscured by the intense absorption ν-(PO_4) band.

The IR spectrum of $CuNi_2(PO_4)_2$ shows two groups of bands. The first set of peaks, located at around 1050 cm^{-1}, could be attributed to the stretching vibration mode of the PO_4 tetrahedra.[24] This band is strongly split in this compound, indicating the presence of highly distorted PO_4 polyhedra in good agreement with the structural results. A band of medium intensity and strongly split also appears at around 600 cm^{-1}, which can be attributed to the PO_4 bending modes, reflecting the distortions observed for the phosphate groups.

ESR Spectroscopy. Powdered X- and Q-band ESR spectra of the intercalated derivative and $CuNi_2(PO_4)_2$ compound were carried out in the range of 4.2−300 K. The spectra of the intercalated compound show a weak and very broad signal that can be attributed to the zero field splitting of the Ni(II) ions in a distorted octahedral geometry. No significant variation with decreasing temperature was observed. The most important result of this study is that signals corresponding to the intercalated Cu(II) ions were not observed in all studied temperature range. This fact can be attributed to the presence of long-range magnetic interactions between the Cu(II) and Ni(II) ions in which the main effect is the corresponding to the Ni(II) ions.[25] The exchange pathway between the magnetic ions is established through the PO_4 groups.[26] Taking into account the ESR results, we can conclude that the distribution of the Cu-(II) ions in the interlayer space is better described as that corresponding to the case (b) in which each Cu(II) is linked to two Ni(II) ions (see Figure 3).

Powdered X- and Q-band ESR spectra for the $CuNi_2$-$(PO_4)_2$ compound were also registered. The X-band spectra performed in the range of 4.2−300 K are shown in Figure 8a. At room temperature, the X-band signal is quasi-isotropic with a g value of 2.354, whereas the Q-band spectrum shows an increase in the anisotropy of the signal with a g value of 2.235. It was not possible to fit the experimental band profile using either Lorentzian or Gaussian curves. The intensity of the signal decreases when the temperature is lowered from 300 to 50 K and maintains a constant value below this temperature. The line width increases in the temperature range of 300−50 K. The band distortion shows a dependence upon T, making the signal more anisotropic at low temperature (Figure 8b). The g_{eff} value also increases when temperature is lowered, reaching a maximum of 2.503 at 10 K (see Figure 8b).

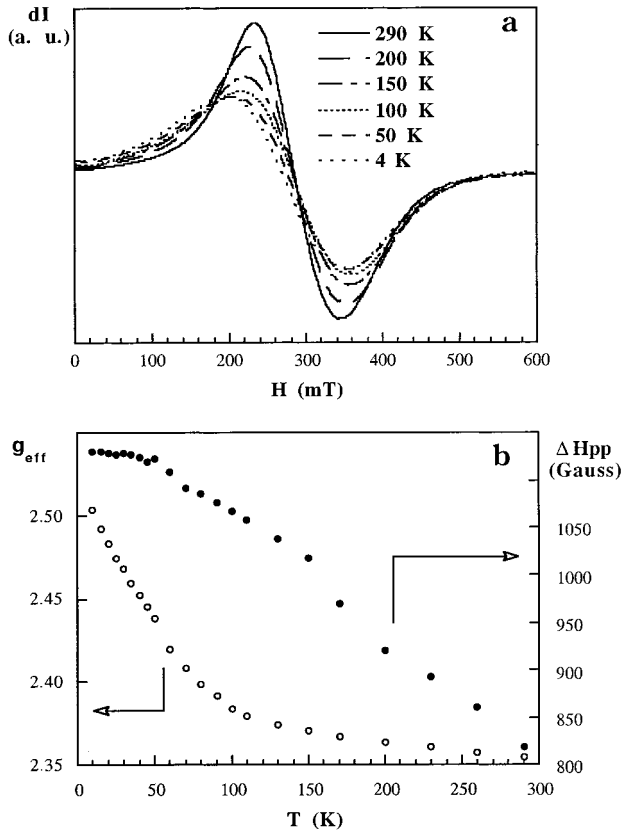

Figure 8. (a) X-band ESR spectra of $CuNi_2(PO_4)_2$ at different temperatures. (b) Thermal evolution of the g_{eff} value and line width, ΔH_{pp}, of the ESR signal.

The results obtained through the anisotropy of the signal, the magnitude of the g_{eff} value and its dependence with the temperature and the experimental microwave frequency indicate that the observed band in the spectra must be attributed to the effect of the two different magnetic ions, Cu(II) and Ni(II), present in the $CuNi_2(PO_4)_2$ compound. The lack of information concerning the ESR spectroscopy of five-coordinated Ni-(II) ions makes the study on this system difficult. However, the presence of the intense signal in the ESR spectrum of $CuNi_2(PO_4)_2$ leads to consider that the zero field splitting effect for this five-coordinated Ni(II) should be smaller than that of the octahedral Ni(II) compounds in which the presence of the D term, in general, gives rise to a very broad absorption at low fields.

The magnetic coupling between two Ni^{2+} and one Cu^{2+} ions originates a complicated magnetic system with an effective spin of $S' = 5/2$, affected by the zero field splitting of the Ni(II) cations. In this way, the experimental ESR band in each spectrum corresponds to the sum of the different allowed signals for each temperature and frequency employed in the measurement. So, we can conclude that the thermal evolution of the spectra and the notable differences of the g_{eff} values are originated by the thermal development of the population of the different energetic terms in the system.

(23) Nakamoto, K. *Infrared and Raman Spectra of Inorganic and Coordination Compounds;* Wiley-Intersciences: New York, 1997.
(24) Rulmont, A.; Cahay, R.; Liegeois-Duyckaerts, M.; Tarte, P. *Eur. J. Solid State Inorg. Chem.* **1991**, *28*, 207.
(25) Bencini, A.; Gatteschi, D. *Electron Paramagnetic Resonance of Exchange Coupled Systems*; Springer-Verlag: Berlin, 1990.
(26) Lezama, L.; Suh, K. H.; Villeneuve, G.; Rojo, T. *Solid State Commun.* **1990**, *79*, 449.

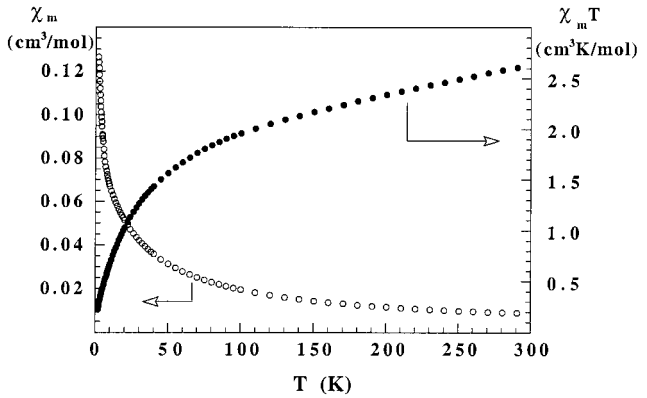

Figure 9. Thermal variation of χ_m and χ_mT for the Cu(II) intercalated derivative.

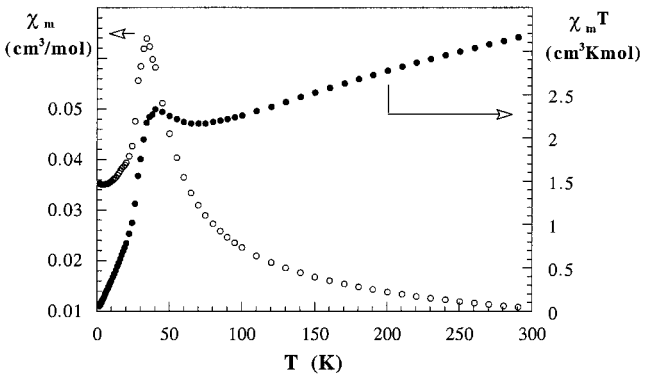

Figure 10. Thermal variation of χ_m and χ_mT for the $CuNi_2(PO_4)_2$ compound.

Magnetic Properties. The molar magnetic susceptibility measurements of both $Cu_{0.9}Ni_2(PO_4)_{1.8}(HPO_4)_{0.2}\cdot 4H_2O\cdot 1.5CH_3OH$ and $CuNi_2(PO_4)_2$ compounds were carried out in the temperature range of 1.8−300 K at 0.1 T magnetic field.

The thermal evolution of χ_m together with χ_mT of the Cu(II) intercalated compound are represented in Figure 9. The χ_m values increase with decreasing temperature in all temperature range, without the presence of any maximum in the curve. This behavior differs from that observed for the rest of the related compounds, such as $NH_4NiPO_4\cdot H_2O$, $HNiPO_4\cdot H_2O$, and the alkylamines intercalated derivatives $(C_nH_{2n+1}NH_2)_xHNiPO_4\cdot H_2O$ in which the χ_m curves showed a maximum at around 10−15 K. The thermal evolution of χ_m for this compound does not satisfy the Curie−Weiss law, included the high-temperature range. Moreover, the χ_mT vs T curve (see Figure 9) shows a continuous fall from 300 to 1.8 K. This fact could be attributed to the effect of the temperature-independent paramagnetism due to the presence of Ni(II) ions in the sample. Notwithstanding, the major contribution must correspond to the antiferromagnetic interactions of long-range order in the compound.

If we consider that, during the intercalation process of the Cu(II) ions between the layers of $HNiPO_4\cdot H_2O$, the structure of the nickel phosphate sheets remain unchanged, as was observed for the alkylamine intercalated phases,[8] one can conclude that the magnetic intralayer interactions in the $Cu_{0.9}Ni_2(PO_4)_{1.8}(HPO_4)_{0.2}\cdot 4H_2O\cdot 1.5CH_3OH$ and the related $HNiPO_4\cdot H_2O$, $NH_4NiPO_4\cdot H_2O$, etc. compounds might be similar. So, the different magnetic behavior observed for the first compound can be considered as originated by further magnetic interactions introduced by the Cu^{2+} ions inserted in the interlayer space. The no existence of any maximum in the χ_m vs T curve could be interpreted as due to the presence of three-dimensional interactions in the Cu(II) intercalated compound. This fact would be in opposition to that observed for the 2D−3D intermediate antiferromagnetic behavior in the $NH_4NiPO_4\cdot H_2O$ and $HNiPO_4\cdot H_2O$ phases in which the interlayer exchange pathways were established only through hydrogen bonds. The absence of structural data prevents establishing the positions of the Cu(II) ions inside the interlayer space of $Cu_{0.9}Ni_2(PO_4)_{1.8}(HPO_4)_{0.2}\cdot 4H_2O\cdot 1.5CH_3OH$. However, taking into account the magnetic behavior and the ESR measurements, the option in which the Cu(II) ions would act as bridges between the layers seems to be the most reasonable. The existence of an effective exchange pathway between layers involving the Cu^{2+} ions makes the intralayer $Ni^{2+}-Ni^{2+}$ antiferromagnetic interactions to be weaker, inducing a decrease in the value of the intralayer coupling constant J. This phenomenon originates a shift of the Neel temperature to lower values, and so, the maximum in χ_m is not observed included at 1.8 K. This result is in good agreement with that observed in the ESR measurements and allows the rejection of the fact that the Cu(II) ions are magnetically isolated between the layers.

The thermal evolution of the molar magnetic susceptibility of $CuNi_2(PO_4)_2$ is shown in Figure 10. The χ_m value increases with decreasing temperature, reaching a maximum at 34 K. An anomaly is observed in the curve at 18 K, which can be attributed to the maximum in the χ_m of the $Ni_3(PO_4)_2$[27] impurity present in the sample, as was detected from crystallographic data. The magnetic behavior of the $CuNi_2(PO_4)_2$ compound does not follow the Curie−Weiss law in the studied temperature range. This fact can be attributed, in part, to the temperature-independent paramagnetism of the sample, but the main cause must be attributed to the presence of magnetic interactions of long-range order, which were detected in the ESR study. The χ_mT values decrease with decreasing temperature; however, a relative minimum is observed at 75 K (see Figure 10), reaching a maximum at around 40 K. Below this temperature a new abrupt drop in the magnetic moment is observed. The descending tendency in the χ_mT vs T curve is indicative of a global antiferromagnetic behavior in $CuNi_2(PO_4)_2$. However, the presence of a maximum in χ_mT at a temperature slightly higher than that of the χ_m maximum could be attributed to many different factors: (i) the existence of a ferromagnetic contribution prevailing during a short temperature range, (ii) the presence of a phenomenon of ferrimagnetism, or (iii) the effect of the zero field splitting corresponding to the Ni(II) ions. This last hypothesis would be the less probable, although curves of similar appearance have been observed for dimers with Ni(II) ions in octahedral geometry.[28] However, in the mentioned dimers the D value was higher than those corresponding to the $CuNi_2(PO_4)_2$

(27) Rojo, T.; Lezama, L.; Rojo, J. M.; Insausti, M.; Arriortua, M. I.; Villeneuve, G. *Eur. J. Solid State Inorg. Chem.* **1992**, *29*, 217.

(28) Nanda, K. K.; Das, R.; Thompson, L. K.; Venkatasubramanian, K.; Pul, P.; Nag, K. *Inorg. Chem.* **1994**, *33*, 1188.

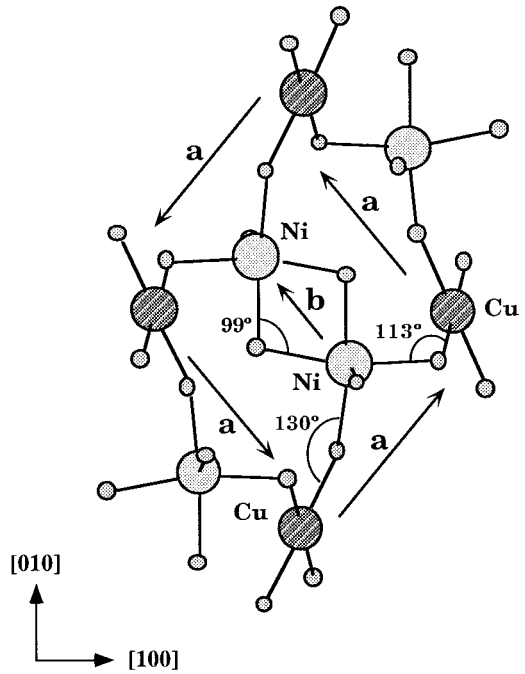

Figure 11. Scheme of the magnetic exchange pathways in the (101) plane for the $CuNi_2(PO_4)_2$ compound.

compound, in which the Ni(II) ions are five-coordinated, and the maxima of the χ_m values were observed in all cases at lower temperatures than 30 K.

To better explain the magnetic properties of the $CuNi_2(PO_4)_2$ compound, two mean intermetallic exchange pathways have been proposed, which are marked by arrows in Figure 11. The magnetic pathway through the (a) direction would run along the (101) plane through the −Cu−O(4)−Ni−O(1)−Cu- heterometallic way. The intermetallic angles show values of 113° and 130°, respectively and, consequently the couplings would be antiferromagnetic. The interactions could take place between the two-half-filled orbitals $d_{x^2-y^2}$ and d_{z^2} of Ni(II) and the homologous orbitals of the Cu(II) ion, which have only one unpaired electron. As the magnetic moment of the Ni(II) ion has theoretically twice the value of that corresponding to the Cu(II) ion, the interactions between these two metallic ions can give rise to the presence of uncompensated spins originating a ferrimagnetic character in this exchange pathway. The magnetic system would be distributed in the plane (101) with alternating $S = 1/2$, $S = 1$ spins and two alternating J values, which are similar in sign but not in magnitude. This fact allows us to explain the behavior of the $\chi_m T$ vs T curve up to the maximum observed at 40 K. Unfortunately, the presence of alternating J values in the system together with the ignorance of the g values for each magnetic cation makes the fit of the experimental curve difficult.

The second magnetic exchange pathway b) would take place inside the Ni_2O_8 dimers, in which the two Ni(II) ions interact through the two shared symmetrical O(2) oxygens. The value of the intermetallic angle of 99° does not allow the prediction of the type of the magnetic interactions present in this pathway. The Ni−Ni distance inside the dimer presents a value of 3.029 Å, and so, any contribution of direct exchange could not be considered in the magnetic structure of this phase.

Finally, a third exchange pathway through the PO_4 groups could be also considered. This fact, similar to that observed in other phosphate compounds,[29] gives rise to the three-dimensional character of this system. As a result, a total cancellation of the magnetic moments takes place establishing the global antiferromagnetic ordering in this system. These exchange interaction pathways are in good agreement with those observed in the related $Cu_3(PO_4)_2$ phase.[30,31]

Concluding Remarks

The intercalated Cu(II) compound, $Cu_{0.9}Ni_2(PO_4)_{1.8}(HPO_4)_{0.2} \cdot 4H_2O \cdot 1.5CH_3OH$, was prepared from the suspension of the $HNiPO_4 \cdot H_2O$ layered phase in a methanolic solution of copper salts. The Cu^{2+} cations together with water and solvent molecules have been intercalated into the host. From structural and ESR data, it can be concluded that the Cu(II) species are acting as bridges between the Ni(II) phosphate layers. The presence of Cu(II) species in the interlayer space allows us to establish three-dimensional antiferromagnetic interactions.

The thermal treatment of the Cu^{2+} intercalated derivative led to the attainment of a new $CuNi_2(PO_4)_2$ phosphate, in which the Ni(II) ions are located in an unusual five-coordinated geometry forming Ni_2O_8 dimers. The Cu(II) ions, in CuO_4 planar square entities, do not present connection between them and are corner-sharing with the Ni_2O_8 dimers. The oxygen atoms of the PO_4 groups act as bridges in the structure. The long-range order of the magnetic coupling between the Ni^{2+} and Cu^{2+} ions originates a complicated magnetic system with effective spin $S' = 5/2$. The observation of the ESR signal in this compound permits us to conclude that the effect of the zero field splitting of the Ni(II) cations is lower than that observed for this cation in an octahedral geometry. The $CuNi_2(PO_4)_2$ phase shows a global antiferromagnetic ordering, with the presence of a ferrimagnetic behavior probably due to the spin decompensation between both types of coupled magnetic ions in the compound.

Acknowledgment. This work has been carried out with the financial support of the Eusko Jaurlaritza-Gobierno Vasco (PI-9439) and the Ministerio de Educación y Ciencia (PB97-0640), which we gratefully acknowledge.

CM980785W

(29) Forsyth, J. B.; Wilkinson, C.; Paster, S.; Wanklyn, B. M. *J. Phys. C.: Solid State Phys.* **1988**, *21*, 2005.
(30) Moqine, A.; Boukhari, A.; Flandrois, S. *Mater. Res. Bull.* **1987**, *22*, 965.
(31) Forsyth, J. B.; Wilkinson, C.; Paster, S.; Effenberger, H. *J. Phys.: Condens. Matter.* **1990**, *2*, 1609.